

Dielectric Gate Applications of PMMA-TiO₂ Hybrid Films in ZnO-Based Thin Film Transistors

C.G. Alvarado-Beltrán¹, J.L. Almaral-Sánchez², M.A. Quevedo-López³ and R. Ramirez-Bon^{1,*}

¹ Centro de Investigación y de Estudios Avanzados del IPN. Unidad Querétaro, Apdo. Postal 1-798, 76001, Querétaro, Qro., México

² Universidad Autónoma de Sinaloa, Fuente de Poseidón y Prol. Angel Flores, S.N., 81200, Los Mochis Sin., México.

³ Department of Materials Science and Engineering, The University of Texas at Dallas, Richardson 75083, TX, USA

*E-mail: rrbon@gro.cinvestav.mx

Received: 18 January 2015 / Accepted: 2 March 2015 / Published: 23 March 2015

In this paper we report a low temperature sol-gel deposition process of organic-inorganic PMMA-TiO₂ hybrid films for applications to gate dielectric layers in field-effect (FE) thin film transistors (TFT), using sputtered n-type ZnO as semiconductor active layer. The PMMA-TiO₂ hybrid thin films were prepared by a modified sol-gel route using titanium butoxide (TBT) as the inorganic (titania) source, methyl methacrylate (MMA) as the organic source, and 3-trimethoxy-silyl-propyl-methacrylate (TMSPM) as the coupling agent between organic and inorganic phases. The hybrid precursor solution for the deposition of the films contained the three precursors with molar ratio 1:0.25:0.25 for TBT, TMSPM and MMA, respectively. For characterization purposes, the hybrid thin films were deposited by dip coating on glass slides substrates and subsequently heat-treated at 100 °C for 24 h. Previous to the device applications, the hybrid films were analyzed by scanning electron microscopy (SEM), atomic force microscopy (AFM), Fourier Transform Infra-Red (FTIR) spectroscopy, transmission and reflection spectroscopy and thermogravimetric analysis (TGA) measurements. The macroscopic characteristics of the hybrid films such as high homogeneity and high optical transparency evidenced the formation of a cross-linked, interpenetrated organic-inorganic network. The dielectric characteristics of the PMMA-TiO₂ hybrid films were studied by measuring capacitance-voltage (C-V) and current-voltage (I-V) curves in metal-insulator-metal (MIM) structures, using gold as metal contacts. Finally, the hybrid films were tested as gate dielectric layers in thin film transistors with structure ZnO/PMMA-TiO₂/ITO/Glass, with a common bottom gate and patterned Al source/drain contacts. We analyzed the output electrical response and transfer characteristics of the hybrid dielectric gate TFTs to determine their performance parameters.

Keywords: hybrid materials; thin films; sol-gel growth; dielectric properties; thin films transistors.

1. INTRODUCTION

The sol-gel synthesis allows for the tailoring of specific properties of organic-inorganic hybrid materials by blending the proper amounts of organic and inorganic components. This process allows the proper linking between the organic and inorganic phases at the molecular level and the adjusting of the degree of interpenetration of both components from sub-micron range to the nano scale level, providing an easy method to synthesize different classes of hybrid materials [1]. Therefore, the possibility of combining properties of organic and inorganic networks in a unique hybrid material has been exploited in the last years for multiple purposes [2]. Several hybrid systems have been reported in literature, most of them prepared by means of the sol-gel process, which allows the synthesis of hybrid materials at room temperature with organic-inorganic molecular-scale interaction yielding to highly homogenous films and nanocomposites [7-10]. Poly methyl methacrylate (PMMA) is an important thermoplastic polymer with excellent transparency, refractive index, $n=1.49$, good chemical resistance, thermal stability, mechanical flexibility, low cost and lower dielectric constant (2.9) than that of thermal silicon oxide material (3.9) [7]. As organic phase in a hybrid system, PMMA has been mixed with others inorganic phases, mainly silicon oxide, to provide high optical transparency, lower weight, mechanical flexibility and formability to the hybrid composite materials. On the other hand, titania (titanium dioxide) with high transparency, good mechanical properties, high dielectric constant, high refractive index of 2.45 (anatase phase) or 2.7 (rutile phase), depending on its crystal structure [1Error! Reference source not found.], is an excellent material to be mixed in a hybrid system with another organic phase such as PMMA. The incorporation of titania bound to PMMA at nanoscale level has been reported for the production of hybrid materials with high refractive index [12-14]. In most of these reports, the PMMA-titania hybrid system is prepared by the sol-gel method and it is constituted by a PMMA matrix with embedded titania nanoparticles [12]. The disadvantage of such hybrid systems is that, depending on the size, the nanoparticles can produce light scattering, even for small size nanoparticles they can agglomerate, yielding to low optical quality materials [13-18]. Therefore, the appropriate incorporation of both organic and inorganic phases in the hybrid network is a very important issue, which defines the most important characteristics of the composite materials. [1, 19].

The increasing interest on organic and flexible electronics has promoted the search for new semiconductors and dielectrics materials, including hybrid organic-inorganic, for applications in electronic devices [6]. The main constrain for these materials is low temperature processing, compatible with the low temperature resistance of the plastic substrates employed in flexible electronics. Regarding dielectric applications, hybrid materials have been also applied in organic electronic devices [20,21]. There are several reports about hybrid dielectric gate layers employed in TFTs, where the hybrid layers correspond to inorganic nanoparticles embedded in polymeric matrix [22-25] or inorganic-organic bilayers [26]. In a recent work we reported the application of PMMA-SiO₂ gate dielectric layers to the fabrication of ZnO-based TFT devices [27]. Particularly, due to their higher dielectric constant, hybrid dielectric gate layers have been able to reduce the operative voltage in ZnO-based TFT devices [20,21,26], which typically have high threshold voltage. The low temperature processing of hybrid materials accomplish the required conditions for the deposition on plastic substrates, therefore, the potential applications of the hybrid materials can be extended to cover

organic flexible electronics [28]. For this, it is important the study of their dielectric properties and how they can be improved to attain dielectric characteristics, such as high dielectric constant and low leakage current, which allow their application in devices such as dielectric layer in capacitors and TFTs [7,27]. The understanding of the phase interaction in the hybrid structure at molecular level, including the influence of chemical groups on the polarizability, is essential to explain the dielectric properties of the hybrid layers. [2]. The PMMA-TiO₂ hybrid system is an attractive alternative dielectric gate material because the high dielectric constant of TiO₂, which value for Rutile phase is 114 [21]. On the other hand, PMMA, with dielectric constant 3.2, has shown to be a good alternative organic dielectric in organic TFT devices (OTFT) [29,30]. Therefore, the proper blend of these organic and inorganic materials in a hybrid material with strong coupling between both phases would be an excellent candidate as dielectric material [28].

In this work, we report the main characteristics, including dielectric ones, of highly transparent PMMA-TiO₂ hybrid films deposited on glass substrates by the sol-gel method and their application as dielectric gate layer in ZnO-based thin films transistors. The strategy to develop these hybrids films is based in our previous experience on the deposition of PMMA-SiO₂ hybrid films, which basically consists in the in situ polymerization of the organic phase during the hydrolysis and condensation of the inorganic one [2,7,19-21]. For this, in addition to organic and inorganic precursors, a coupling agent to improve the compatibility between both phases and enhance their interaction at the interface level was included among the precursor reagents [31]. Unlike most of the papers on this hybrid system, the kind of hybrid material that we attain is Class II type, that is, the linking between organic and inorganic phases is through strong covalent chemical bonding. The properties of the hybrid films reflect such strong phases interaction. In this study, we report first the low temperature deposition process of the PMMA-TiO₂ gate dielectric layers and the analysis of their structural, optical and dielectric properties determined from several experimental techniques. Also, it is reported the fabrication process of the TFT devices with PMMA-TiO₂ and ZnO as the hybrid dielectric gate and semiconductor layers, respectively, and the analysis of the electrical output and transference characteristics to determine their performance electrical parameters.



Figure 1. Photograph showing the image of the homogeneous and highly transparent PMMA-TiO₂ hybrid films.

2. EXPERIMENTAL DETAILS

The sol-gel method to prepare the hybrid PMMA-TiO₂ films was based on a similar method for the deposition of PMMA-SiO₂ films previously described in several reports by our group [2,7,21]. In this work, titanium butoxide (TBT) was used as the inorganic precursor, methyl methacrylate (MMA) as the source of the organic component and 3-trimethoxy-silyl-propyl-methacrylate (TMSPM) as the coupling agent to improve the compatibility between the organic and inorganic phases. The MMA polymerization was initiated with benzoyl peroxide (BPO). Ethyl alcohol and HNO₃ were used as solvents to hydrolyze the inorganic TBT precursors. For the coupling agent it was used HCl and deionized water. The hybrid precursor solution was obtained by mixing the precursor solutions with molar ratio TBT: TMSPM: MMA (1.0: 0.25: 0.25). The resulting homogeneous hybrid solution was used to obtain the hybrid films by dip-coating on conventional glass slide substrates, which were previously cleaned. The substrates were ultrasonically cleaned in acetone, isopropyl alcohol and deionized water for 5 minutes and finally dried with nitrogen. The immersion and removal velocity of the substrates during the dipping process was 10 cm/min. After deposition, the hybrid films were baked for 24 hrs in a conventional oven at 100 °C and atmospheric pressure. After cured the hybrid films were homogeneous, very well-adhered to the glass substrates and highly transparent, as can be observed in the photograph shown in Fig. 1. The hybrid samples were characterized by Fourier transform infrared (FTIR), thermo gravimetric analysis (TGA), scanning electron microscopy (SEM), atomic force microscopy (AFM) and optical transmission (T) and reflection (R) spectroscopy measurements. The FTIR measurements were conducted using a Gx Perkin Elmer system in the reflectance mode (GA-ATR) mode with a resolution of 4 cm⁻¹, in the wave number range of 400-4000 cm⁻¹. For these measurements, the hybrid samples were deposited on Cr/Au (10/100 nm) coated glass substrates. Top view and cross sectional SEM images of the hybrid films were measured in a Zeiss Supra-40. For this, the samples were previously coated with gold. The AFM measurements were done in tapping mode with a Di-Vecco Nanoscope IV instrument. The TGA experiments were performed using a Mettler Toledo Instruments (TGA-851), from room temperature to 1100°C under synthetic air flow (50 ml/min) using a heating rate of 10°C/min. The measurements were carried out using PMMA-TiO₂ powders obtained by using the same temperature and baking time conditions used for the curing of thin films. The T and R spectra the hybrid films were measured using a thin film metrology system (FilmTek TM 3000, Scientific Computing International, Inc) at normal incidence in the UV-visible spectral range (240-840 nm).

For the dielectric characterization of the PMMA-TiO₂ layers, MIM structures were fabricated by depositing the hybrid layers on gold-coated glass substrates and evaporating gold layers (100 nm) as top electrodes using a shadow mask to define top circular contacts (50, 100, 200, 300 and 500 μm diameters). Electrical characteristics were measured using a parameter analyzer (HP4284A, Hewlett Packard) and a C-V analyzer (Keithley 4200). Low and high frequency C-V acquisitions (from 1 KHz to 1MHz) were performed. Currents versus voltage curves of the MIM structures were measured at room temperature with a 4200 Keithley semiconductor parameter analyzer. The TFT devices were fabricated by depositing the PMMA-TiO₂ dielectric films on ITO-coated glass substrates previously cleaned in the same way as the glass substrates. Subsequently, the n-type ZnO thin film (40 nm), as

active semiconductor layer, was deposited by RF sputtering using a commercially sintered ZnO target (99.999%). The RF sputtering process was carried out at room temperature using 50 W of power. Finally, the source and drain electrodes were patterned by thermal evaporation of Al (100 nm) through a metallic shadow mask. The width of the electrodes and channel length of the devices were 500 and 40 μm , respectively. These device processing steps were performed under clean room environment (US-class 10,000). The electrical characteristics of the TFT devices were determined from current-voltage (I-V) measurements at room temperature using a 4200 Keithley semiconductor parameter analyzer.

3. RESULTS AND DISCUSSION

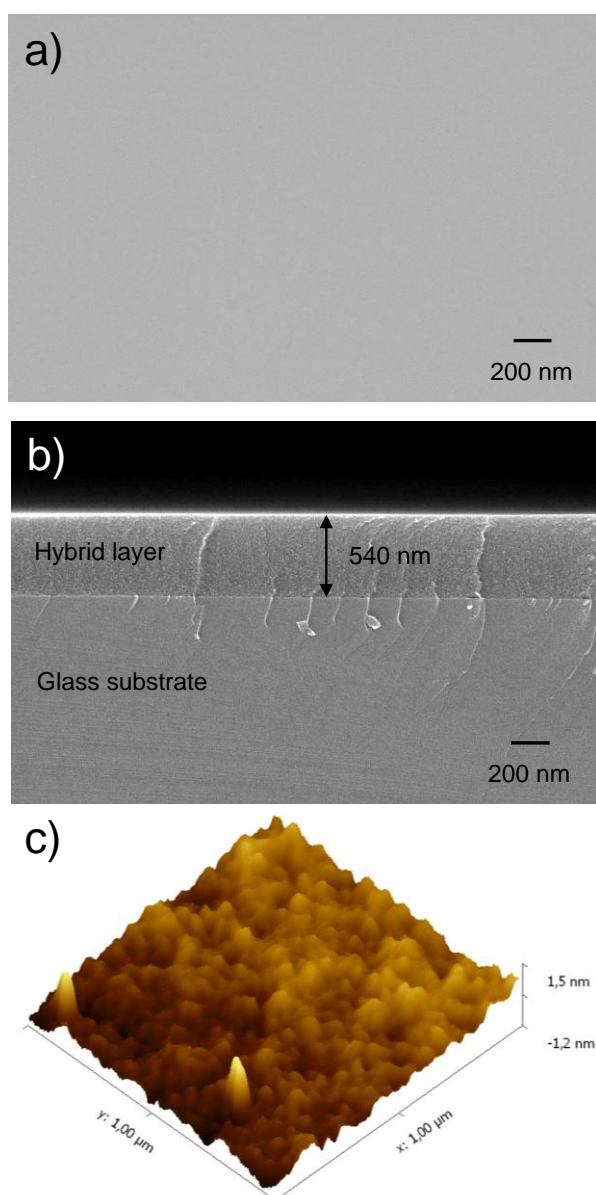


Figure 2. a) Top view b) cross sectional SEM images and c) 3-D AFM image of the PMMA-TiO₂ hybrid film.

Figure 2 display the top view a) and cross sectional b) SEM images and c) 3-D AFM image of the PMMA-TiO₂ hybrid film. As observed in these images, the surface of the hybrid film at this microscopic level is uniform, defect-free, flat and very smooth. The cross sectional image also shows that the hybrid film is very well adhered to the substrate; it has transversal homogeneity with uniform thickness. The measured average thickness of the hybrid film determined from this image is 328 nm. The root mean square (rms) roughness of the film determined from the 1 μm x 1 μm AFM image in c) is 0.36 nm, which is a very low surface roughness value evidencing the smoothness of the hybrid film surface. The surface morphology features in this AFM images have size of tens of nm with distance between highest and lowest heights of the order of 1 nm. These results are consistent with the macroscopic homogeneity and optical transparency of the hybrid films, which can be attributed to the lack of separated phase precipitation at this nanometric scale. Thus, the surface and cross sectional morphology of the hybrid film supports the formation of a homogeneous mixed organic-inorganic network with very small domains in the nanometric scale [1].

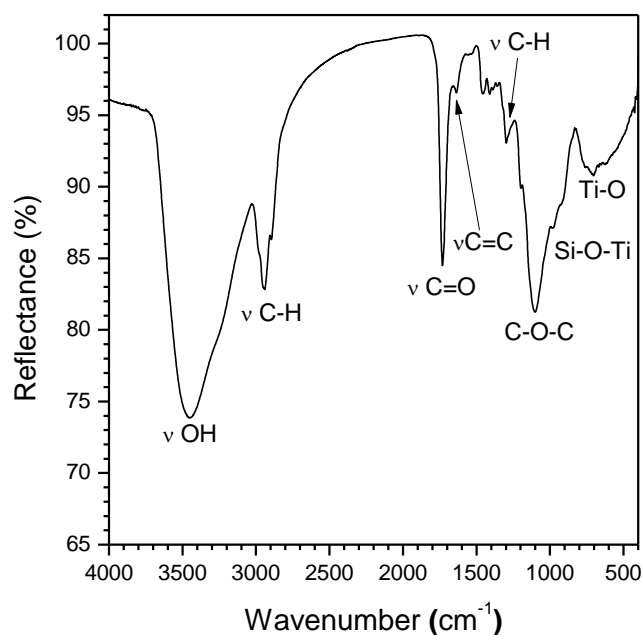


Figure 3. FTIR reflection spectrum of the PMMA-TiO₂ hybrid film.

The chemical groups in the PMMA-TiO₂ hybrid films were identified in its FTIR spectrum shown in Fig. 3, where the most evident absorption bands are labeled with their corresponding vibration modes. The wide and strong band centered at about 3350 cm⁻¹ is attributed to O-H stretching modes [11,13], which are mainly due to Ti-OH groups resulting from the incomplete condensation in the sol-gel process [14,31]. Hydroxyl groups can also adsorb to the surface and have been observed in the FTIR spectra of crystalline TiO₂ [9,10]. The broadness of the band from 3000 to 3600 cm⁻¹ is characteristic of sol-gel materials and it is due to the different interaction forces between the compounds originating a wide variation of the corresponding vibration modes. The absorption bands at

2945, 1730 and 1640 cm^{-1} are due to the PMMA organic phase produced by the stretching vibration modes of C-H, C=O and C=C groups, respectively. The C=C groups are contained in the coupling agent and monomer molecules and it is the bonding point for the polymerization by free radicals [9]. Therefore, this band evidences some incomplete polymerization of the monomer [2,9]. At lower wavenumber, the broad absorption band between 950 and 1230 cm^{-1} is caused by the overlapping of several vibration modes; at 1075 cm^{-1} there is a band assigned to Si-C bonds from the coupling agent molecules [9,11,15], at 1060-1100 cm^{-1} there is another band due to C-O-C stretching vibration modes of the acrylic group [16-18], at 1126 cm^{-1} there is a band assigned to Ti-O-C evidencing some incomplete hydrolysis of TBT and at 930 cm^{-1} there has been reported absorption due to vibration modes of Si-O-Ti groups from the interaction between the inorganic phase and the organic one through the coupling agent molecule [11,14,16,17,31]. The signal observed at 650 cm^{-1} can be related with the vibration modes of the Ti-O-Ti groups [9,12,14] indicating the formation of TiO_2 in the hybrid material. The FTIR analysis provides some insight about the reaction mechanism which allows the formation of the hybrid network. At the beginning, the hydrolysis of TMSPM molecules originates Si-OH groups, which can bind with the Ti-OH groups of the inorganic precursor yielding to the formation of Si-O-Ti groups [9,16,31] and then Ti-O-Ti ones. The condensation from the relatively fast hydrolysis produced by the high reactivity of the inorganic precursor (TBT) in the aqueous medium favors the growth of the inorganic amorphous network constituted by Ti-O-Ti groups [17]. On the other hand, the hydrophobicity of the organic molecules produces the isolated growth of polymeric chains. The free radicals method allows the polymerization by breaking the C=C groups of the monomer molecules and binding to one extreme of the coupling agent molecules with some selectivity due to the hydrophobicity. The other extreme of the coupling agent molecule which is hydrolyzed has affinity for the inorganic component.

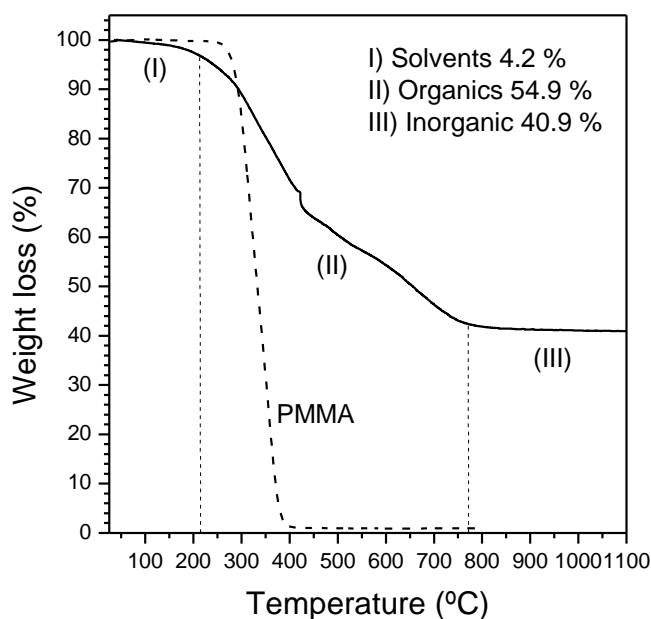


Figure 4. Thermal decomposition graph of the PMMA- TiO_2 hybrid film (solid line) and PMMA material (dashed line).

Figure 4 shows the thermal decomposition of the PMMA-TiO₂ hybrid films (solid line) and for comparison that of PMMA material (dashed line). Three temperature zones, which were labeled as I, II and II, can be identified in this graph. In the 25-230 °C temperature range, zone I, it is observed a no oxidative degradation where the weight loss is due to the release of residual solvents from the hybrid network. The small weight loss at this stage is of 4.17 %. In the zone II, between 230 and 800 °C, it is observed the major and most abrupt weight loss with two different slopes beginning at about 230 and 400 °C, respectively. The first weight drop is associated with the oxidative degradation of PMMA and the second one is due to the degradation of the portion of polymer chains which require higher energy to break [8,12]. On the other hand, the thermal decomposition of PMMA starts at about 270 °C and finish at about 385 °C. The thermal behavior of the hybrid film at this temperature zone shows the better thermal stability of the PMMA phase in the hybrid film as compared with isolated PMMA. It has been reported that pure PMMA start the thermal decomposition at about 245°C with complete weight loss at about 350 °C [11]. In the case of PMMA in the hybrid film, about half its weight is lost at about 400 °C and the other half with higher interaction is lost up to about 800 °C. The improved thermal stability of PMMA is due to the interaction of the polymer chains with the inorganic network of titania which encloses them and limits their movement. At temperatures higher than 800 °C, zone III, the weight of the hybrid film stabilizes at about 41 %. Because the solvents and organic phase have been completely removed at this range of temperature, the remaining of the hybrid sample corresponds to the inorganic part. Based on this analysis the weight content (%) of each phase and remaining solvents in the hybrid film was estimated and the results are shown in the inset of Fig. 4.

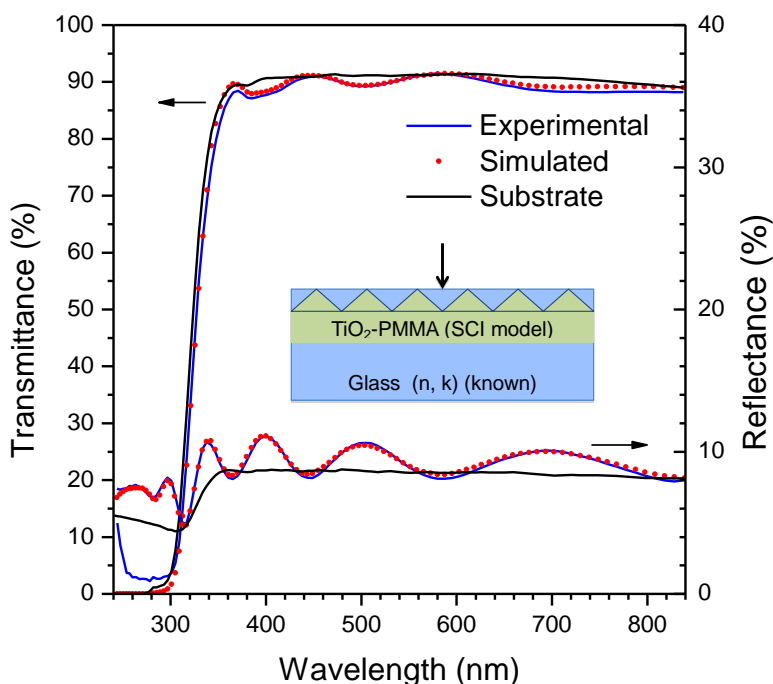


Figure 5. Optical transmittance (T) and reflectance (R) spectra of the PMMA-TiO₂ hybrid film. The solid lines correspond to the measured R and T spectra and the dotted lines are the best fitting to the proposed theoretical model. The inset shows the scheme of the layers model

Figure 5 shows the optical transmission (T) and reflection (R) spectra of the PMMA-TiO₂ films and also for comparison the spectrum of the glass substrate. It is observed that hybrid films are highly transparent in the visible region with average T value of ~90 %, of the same order as that observed in the substrate spectrum. The sharp cut-off of the transmission spectrum at about 340 nm is due to the optical absorption of the glass substrate. It can be also observed interference oscillations in both spectra. The oscillations of the T spectrum lie below the substrate T spectrum with maximum values at points coinciding with the T curve of the substrate. On the other hand, the oscillations of the R spectrum are above the R substrate spectrum with minimum values at points coinciding with the R curve of the substrate, approximately.

These features in the optical spectra are indications of the high optical quality of the hybrid film and that it has higher refraction index than the glass substrate. Furthermore, it is also observed in these optical spectra that R+T values in the transparent region are very close to 100%, showing that the PMMA-TiO₂ film is non-absorbing and the light scattering is negligible. The high optical transparency of the hybrid films prove the formation of a homogeneous composite material with cross-linked organic and inorganic phases, in which the domain have nanometric dimensions much smaller than the wavelength of light in the visible region [31]. Additional information was obtained from the optical spectroscopy measurements, particularly the thickness, refraction index, n , and extinction coefficient, k , of the hybrid films, as a function of wavelength. For this, the T and R spectra of the hybrid film were fit to a theoretical model consisting in two layers representing the hybrid film and the glass substrate, respectively and a roughness external layer.

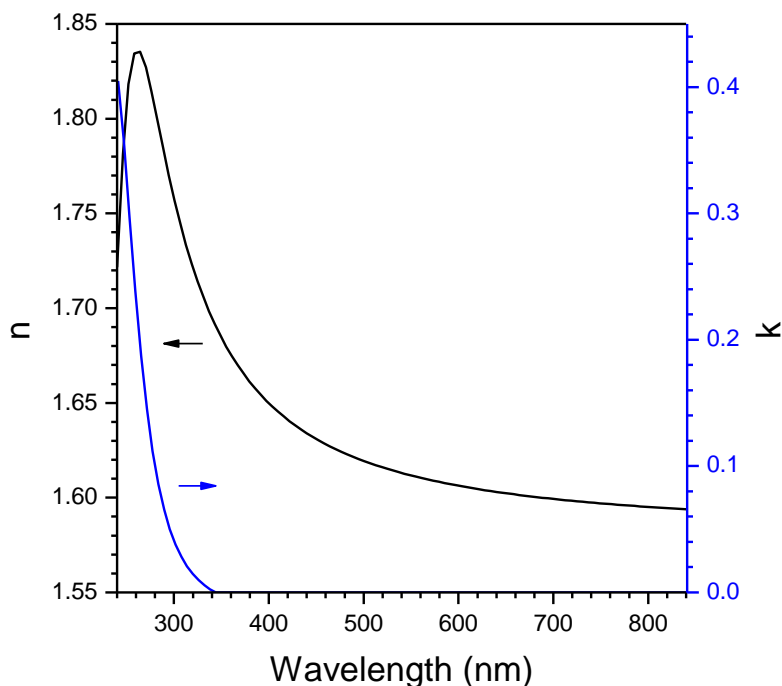


Figure 6. Optical constant n and k of the PMMA-TiO₂ hybrid material as a function of wavelength.

The scheme of the theoretical model is shown in the inset of Fig. 5. The optical constants of the hybrid film were represented by a dispersion relation which is a generalized version of the Lorentz Oscillator Model and the roughness layer was modeled by an effective medium approximation (50 % hybrid film and 50 % air voids), as described in reference [2]. The best fit of this model is plotted as dotted line in Fig. 5 and it shows good agreement with the experimental data over the full wavelength range.

The film thickness determined from this fit is 528 nm, which fairly agrees with the thickness measured from the cross sectional SEM image (Fig. 2 b). The optical constant, n and k , obtained also from the fit, as a function of the wavelength are plotted in Fig. 6. The refractive index increases slightly when wavelength decreases, from 1.6 at 800 nm to about 1.65 at 400 nm. This is a typical behavior of transparent materials in the visible region. The abrupt increase of n at about 340 nm is related with the optical transitions at the fundamental absorption edge of TiO_2 , which is the onset for the increasing of the extinction coefficient k . The optical constants n and k are not independent, they are related by the Kramers-Kronig transformations, and therefore the increase of n in this spectral region is associated with the increase of k . The refractive index of the hybrid film at 532 nm is $n = 1.61$, much higher than that of the organic phase, $n = 1.42$, and other hybrid films [2,14] but lower than that reported for TiO_x amorphous films deposited by sol-gel and annealed at 100 °C, $n = 1.91$. In reference [18] reported $n=1.63-1.68$ for hybrid PMMA- TiO_2 films where the wt % of TiO_2 nanoparticles is 40 %, however it is observed light scattering due to the nanoparticles agglomeration. On the other hand, the extinction coefficient is zero in the visible region and the abrupt increase at 340 nm is produced by the absorption of light of the inorganic phase, that is, it corresponds to the absorption edge of TiO_2 amorphous component in the hybrid film, with energy band gap in the range 3.2-3.5 eV.

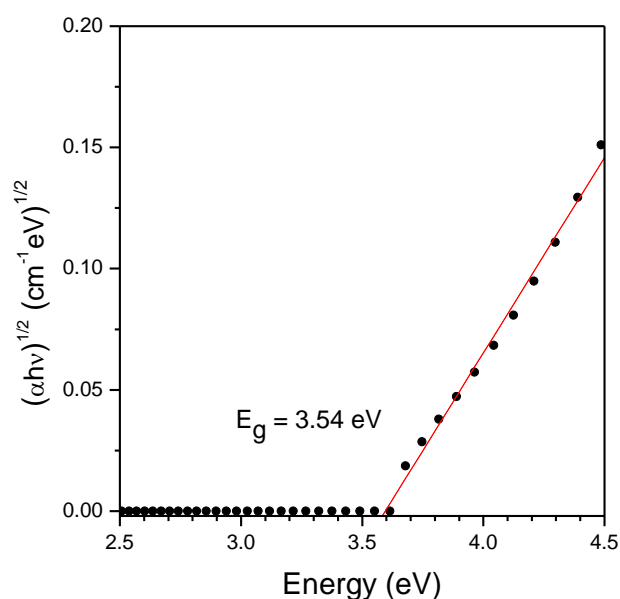


Figure 7. $(\alpha h\nu)^{1/2}$ vs E plot of the PMMA- TiO_2 hybrid material in the TiO_2 absorption edge region. The straight line is the best linear fit in this energy region.

This is because the energy gap reported for PMMA, the organic phase, is 4.6 eV and therefore the absorption of light by this phase is at even lower wavelength. The energy band gap of the inorganic phase was determined by calculating the absorption coefficient spectrum, $\alpha(\lambda)$, of the hybrid films by using the relation $\alpha(\lambda) = 4\pi k / \lambda$ and plotting $(h\nu\alpha)^{1/2}$ vs. E , where h is the Planck constant and ν and E are the frequency and photon energy, respectively. This plot is shown in Fig. 7. According to the Tauc model [18] for fine particles (amorphous materials or nanostructured) the behavior of this plot in the region of the absorption edge must be linear. The linear fit to the experimental data is shown as solid line in this graph and its intersection with the E -axis determines the energy band gap, according to the Tauc model. Therefore, the energy band gap of the TiO_2 inorganic component of the hybrid film is 3.59 eV, slightly higher than the values reported for bulk material in the range 3.2-3.5 eV. This increase could be due to the reduced size of the TiO_2 domains in the hybrid film as shown in the AFM image (Fig. 2 c).

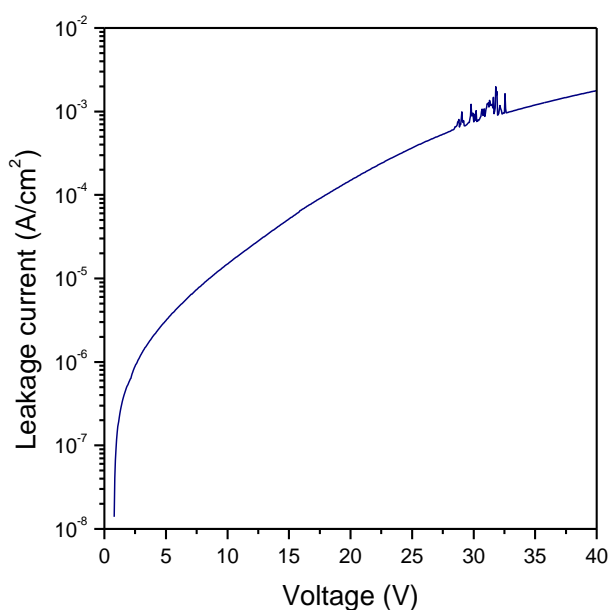


Figure 8. Current versus voltage measured in the MIM structures with PMMA- TiO_2 hybrid dielectric layer.

Figure 8 displays the I - V characteristic curve of the MIM structure measured in the voltage range of 0-40 V. It is observed that the leakage current density is ranging from 10^{-8} to 10^{-3} A/cm² in the entire voltage range. There is no observed dielectric breakdown of the hybrid layer in this curve, even at the highest voltage. From the C - V measurements (not shown) of the MIM structures it was calculated the dielectric constant of the hybrid layers by substituting the value of C , measured at 1 MHz, in $C = \kappa\epsilon_0 A/d$, where κ is the dielectric constant, ϵ_0 , the permittivity of free space, A is the area of the capacitor and d is the thickness of the hybrid dielectric layer. The dielectric constant of the PMMA- TiO_2 layer was 9.2 at 1MHz.

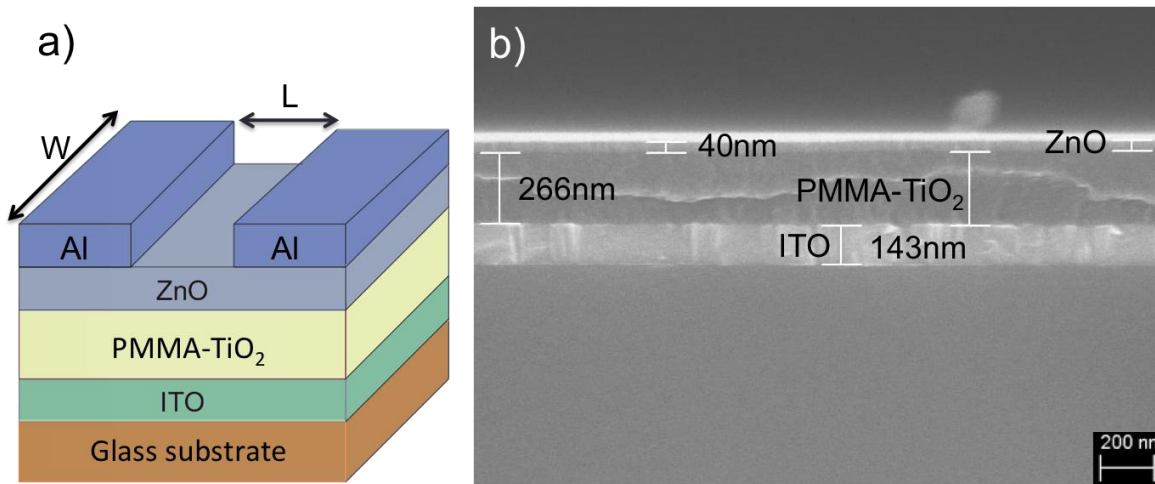


Figure 9. Current versus voltage measured in the MIM structures with PMMA-TiO₂ as the hybrid dielectric layer.

Figure 9 a) is the schematic cross-section of the bottom-common hybrid dielectric gate ZnO-based TFT configuration, meanwhile Fig. 9 b) is the corresponding SEM image of the device cross section, where all the constituting layers and their dimensions in the stack are clearly observed (except Al source and drain). The electrical behavior of the hybrid dielectric gate TFT devices was analyzed from drain-source current (I_{ds}) versus drain-source voltage (V_{gs}) family curves and drain-source current versus drain-source voltage (V_{gs}) transfer characteristics.

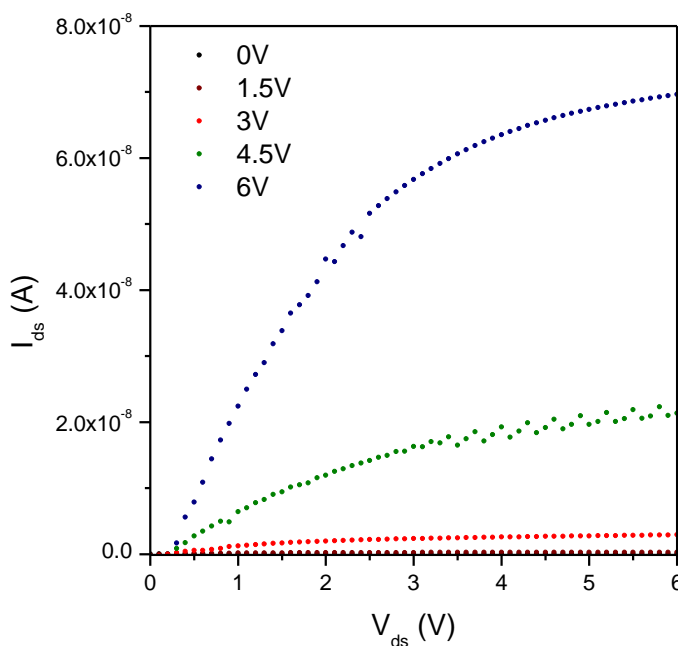


Figure 10. Family of I_{ds} versus V_{ds} curves of the TFT device with PMMA-TiO₂ hybrid dielectric gate layer.

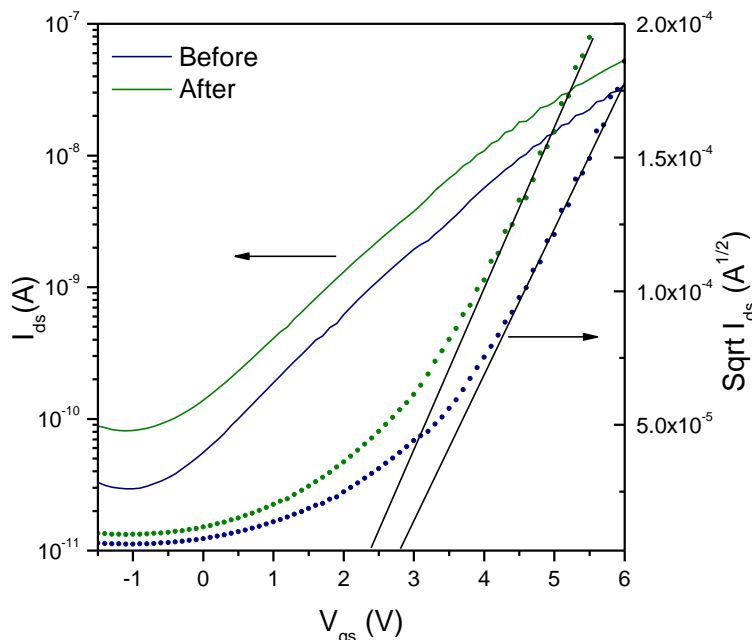


Figure 11. I_{ds} versus V_{gs} (left-axis) and $Sqrt I_{ds}$ versus V_{gs} (right-axis) curves of the TFT device with PMMA-TiO₂ hybrid dielectric gate layer.

Figure 10 shows the I_{ds} - V_{ds} family curves measured at several V_{gs} values, in the range of 0-6 V in steps of 1.5 V. These graphs show the typical electrical response with good current saturation of a TFT device with n -channel, as expected due to the electrical conductivity of the sputtered ZnO active layer. It is observed the linear behavior of the current at low voltages and current saturation at higher voltages. The maximum value of I_{ds} , 7×10^{-8} A, is attained at $V_{ds}=V_{gs} = 6$ V. Figure 11 displays the transfer characteristics of the hybrid dielectric TFT device where the left axis corresponds to I_{ds} in log scale and the right axis to the square root ($Sqrt$) of I_{ds} , as a function of V_{gs} . It is observed in the I_{ds} - V_{gs} curves that the current when the TFT is off, I_{off} , is of the order of 10^{-11} A, meanwhile the current when the TFT is on, I_{on} , increases up to the order of 10^{-8} A, defining an I_{on}/I_{off} current ratio of the order of 10^3 for this device. From the $Sqrt I_{ds}$ versus V_{gs} curves, the saturation mobility (μ_{sat}) and the threshold voltage (V_T) in the saturation region of the devices were determined from linear fits to Equation (1):

$$I_{ds}^{1/2} = \left(\frac{WC_H \mu_{FE}}{2L} \right)^{1/2} (V_{gs} - V_T) \tag{1}$$

where W and L are width and length of the channel, C_H is the capacitance per unit area of the PMMA-TiO₂ hybrid dielectric gate layer, and V_{gs} is the gate-source voltage. The fits to this equation are shown as solid lines in the $Sqrt I_{ds}$ versus V_{gs} curves. The values of saturation mobility and threshold voltage for this device are $0.09 \text{ cm}^2/\text{Vs}$ and 2.8 V , respectively. The positive value of threshold voltage indicates that the TFT device operates in the enhancement-mode, which is an important advantage for low power consumption. In this operating mode, at $V_{gs}=0 \text{ V}$ the device is in the off-state and a positive gate bias is required to form a conductive channel. Therefore, the low threshold voltage measured in our hybrid dielectric gate device is very convenient and it is rather low compared to those measured in other ZnO-based devices [27,28,32] and other OTFT using a hybrid

dielectrics [23]. On the other hand, the value for the mobility is similar to other values reported in literature for ZnO-based TFTs [28,32]. The electrical parameters determined for this hybrid dielectric gate TFT device, as well as the dielectric constant of the hybrid layer, are shown in table 1. The before and after labels in Fig. 11 refer to two consecutive measurements of the I_{ds} - V_{gs} curves. The observed V_{gs} shift to lower values in the curves is produced by some charge trapping at the dielectric-semiconductor interface. However, the shift is small evidencing that the charge trapping effects are not so important. These results describing the electrical behavior of the ZnO-based TFT device employing PMMA-TiO₂ thin films, processed by sol-gel at low temperatures, show that the hybrid dielectric layers have a good performance as dielectric gate. The proper shape of the family curves showing good current saturation and of the transference characteristics with good contrast between the off and on-current states, are clear evidences that the polarization of the hybrid dielectric gate is capable to modulate the current in the semiconductor channel of the device.

4. CONCLUSIONS

In this work we have successfully applied a low temperature sol-gel method to deposit PMMA-TiO₂ hybrid films on glass substrates. The results show that the hybrid films are constituted by a homogeneous organic-inorganic cross-linked network with domain size in the nanometric level, with macroscopic appearance of high optical transparency and uniformity. The strong interaction between organic and inorganic phases is supported by the FTIR, TGA and T and R spectroscopy measurements. SEM and AFM images of the hybrid films show a uniform, smooth and very flat surface with average roughness lower than 1 nm. The dielectric characteristics of the PMMA-TiO₂ layers with dielectric constant 9.2 and leakage current of the order of 10⁻⁸ A at low voltage were considered appropriate to the hybrid layer as dielectric gate in TFT devices. The TFT devices with structure ZnO/PMMA-TiO₂/ITO/Glass showed the proper electrical behavior in the enhancement mode, with saturation mobility of 0.09 cm² V⁻¹ s⁻¹, low threshold voltage of 2.8 V and on-off current ratio of 10³. The low operating voltage of these devices, with mobility similar to other ZnO-based devices, show that the PMMA-TiO₂ hybrid material, processed at 100 °C, is a good candidate as dielectric material, to be used in flexible electronics applications.

ACKNOWLEDGEMENTS

The technical assistance of R.A. Mauricio-Sánchez, C.A. Ávila-Herrera, J.E. Urbina-Alvarez and M.C. Delgado-Cruz is gratefully acknowledged.

References

1. M. F. Ashby and Y. J. M. Bréchet, *Acta Mater*, 51 (2006) 5801.
2. M. D. Morales-Acosta, C. G. Alvarado-Beltrán, M. A. Quevedo-Lopez, B. E. Gnade, A. Mendoza-Galván, R. Ramírez-Bon, *J. Non-Cryst. Solids*, 362 (2013) 124.
3. A. Fidalgo and L. M. Ilharco, *J Non-Cryst Solids*, 283 (2001) 144.

4. P. Innocenzi. *J Non-Cryst Solids*, 316 (2003) 309.
5. J. Wen and G. L. Wilkes, *Chem. Mater.* 8 (1996) 1667-1681.
6. C. Sanchez, B. Lebeau, F. Chaput and J. P. Boilot, *Adv. Mater.* 15 (2003) 1969.
7. M. D. Morales-Acosta, M. A. Quevedo-Lopez, B. E. Gnade and R. Ramirez-Bon, *J. Sol-Gel Sci. Techn.* 58 (2011) 218.
8. Jianwen Xu, Wenfang Shi, Ming Gong, Fei Yu, Lifeng Yan, *J. Appl. Polym. Sci.* 97 (2005) 1714.
9. A. H. Yuwono, B. Liu, J. Xue, J. Wang, H. I. Elim, W. Ji, Y. Li and T. J. White, *J. Mater. Chem.* 14 (2004) 2978.
10. C. Deng, P. F. James and P. V. Wright. *J. Mater. Chem.* 8 (1998) 153.
11. H. C. Kuan, S. L. Chiu, C. H. Chen, C. F. Kuan and C. L. Chiang, *J. Appl. Polym. Sci.* 113 (2009) 1959.
12. N. Nakayama and T. Hayashi, *J. Appl. Polym. Sci.* 105 (2007) 3662.
13. Y. Tong, Y. Li, B. F. Xie and M. Ding, *Polym. Int.* 49 (2000) 1543.
14. B. Wang and L. Hu, *Ceram. Int.* 32 (2006) 7.
15. X. Zhang, J. Yang, Z. Zeng, L. Huang, Y. Chen and H. Wang, *Polym. Int.* 55 (2006) 466.
16. D. Koziej, F. Fischer, N. Kränzlin, W. R. Caseri and M. Niederberger, *ACS Appl. Mater Interfaces*, 1 (2009) 1097.
17. G. Gu, Z. Zhang and H. Dang, *Appl. Surf. Sci.* 221 (2004) 129.
18. A. H. Yuwono, Y. Zhang, J. Wang, X. H. Zhang, H. Fan and J. Wei, *Chem. Mater.* 18 (2006) 5876.
19. J. L. Almaral-Sánchez, E. Rubio, A. Mendoza-Galván, R. Ramirez-Bon. *J. Phys. Chem. Solids*, 66 (2005) 1660.
20. C. G. Choi and B. S Bae, *Synthetic met.* 159 (2009) 1288.
21. F. C. Chen, C. S. Chuang, Y. S. Lin, L. J. Kung, T. H. Chen and H. P. D. Shie, *Org. Electron.* 7 (2006) 435.
22. J. Kim, S. H. Lim and Y. S. Kim, *J. Am. Chem. Soc.* Vol. 132. No. 42 (2010) 14721.
23. W. H. Lee, C. C. Wang and J. C. Ho, *Thin Solids Films*, 517 (2009) 5305.
24. F. Y. Yang, M. Y. Hsu, G. W. Hwang and K. J. Chang, *Org. Electron.* 11 (2010) 81.
25. C. T. Liu, W. H. Lee and J. F. Su, *Act. Passive Electron. Compon.* 2012 (2012) 1.
26. S. H. Cha, M. S. Oh, K. H. Lee and S. Im, B. H. Lee and M. M. Sung, *Appl. Phys. Lett.* 92 023506 (2008) 1.
27. M. D. Morales-Acosta, M. A. Quevedo-López and R. Ramirez-Bon, *Mater. Chem. Phys.* 146 (2014) 380.
28. H. C. You and Y. H. Lin, *Int. J. Electrochem. Sci.* 7 (2012) 9085.
29. T. G. Kim, E. H. Jeong, S. C. Lim, S. H. Kim, G. H. Kim, H. Y. Jeon and J. H. Youk, *Synthetic Met.* 159 (2009) 749-753.
30. M. Estrada, I. Mejia, A. Cerdeira, B. Iñiguez, *Solid State Electron.* 52 (2008) 53.
31. L. H. Lee and W. C. Chen, *Chem. Mater.* 13 (2001) 1137.
32. H. C. You, *Int. J. Electrochem. Sci.* 8 (2013) 9773.